

KEK-TH-530

hep-ph/9708227

August 1997

## Pseudoscalar pole terms in the hadronic light-by-light scattering contribution to muon $g - 2$

M. Hayakawa<sup>1</sup> \* and T. Kinoshita<sup>2</sup> †

<sup>1</sup> *Division of Theoretical Physics, KEK,*

*Tsukuba, Ibaraki, 305 Japan*

<sup>2</sup> *Newman Laboratory, Cornell University,*

*Ithaca, New York, 14853 USA*

(September 23, 1997)

### Abstract

The pseudoscalar pole contribution is the dominant source of the  $\mathcal{O}(\alpha^3)$  hadronic light-by-light scattering effect in muon  $g - 2$ . We have examined this contribution taking account of the off-shell structure of the pseudoscalar-photon-photon anomaly vertex deduced from available experimental data. Our work leads to an improved estimate,  $-79.2 (15.4) \times 10^{-11}$ , for the total hadronic light-by-light scattering contribution to the muon  $g - 2$ .

PACS numbers: 13.40.Em, 14.60.Ef, 12.39.Fe, 12.40.Vv

Typeset using REVTeX

---

\* Electronic address: hayakawa@theory.kek.jp

† Electronic address: tk@hepth.cornell.edu

## I. INTRODUCTION

New measurement of the anomalous magnetic moment of the muon (muon anomaly)  $a_\mu = \frac{1}{2}(g_\mu - 2)$  is underway at Brookhaven National Laboratory [1]. The anticipated level of precision,  $40 \times 10^{-11}$ , is more than 20 times higher than that of the best previous result [2]

$$a_\mu(\text{exp}) = 1\,165\,923\,(8.5) \times 10^{-9}, \quad (1.1)$$

where the numerals in parentheses represent the uncertainties in the last digits of the measured value. The primary purpose of the new muon  $g - 2$  experiment is to verify the presence of the electroweak contribution. Other effects of potential interest are those of supersymmetric particles [3,4] and leptoquarks [5,6].

At present the standard model prediction of  $a_\mu$  is

$$a_\mu(\text{th}) = 116\,591\,714\,(96) \times 10^{-11}. \quad (1.2)$$

This consists of five parts:

(i) Pure QED contribution <sup>1</sup>

$$a_\mu(\text{QED}) = 116\,584\,705.7\,(1.9) \times 10^{-11}. \quad (1.3)$$

(ii) Hadronic vacuum polarization contribution obtained mainly from the measured hadron production cross section in  $e^+e^-$  collisions [9–12]. We quote here the latest evaluation that includes additional information obtained from the analysis of hadronic tau decay data [13,14]:

---

<sup>1</sup> Eq. (1.3) is obtained from the measured value of the electron anomaly  $a_e$  [7] *minus* a small correction to  $a_e$  due to muon, hadron, and weak interactions [8], *plus* the terms of  $a_\mu$  dependent on the electron and tau masses evaluated using the fine structure constant obtained from the electron anomaly [8].

$$a_\mu(\text{had.v.p.}) = 7\,011 (94) \times 10^{-11}. \quad (1.4)$$

(iii) Higher order hadronic vacuum polarization effect [15]:

$$a_\mu(\text{higher had.v.p.}) = -101 (6) \times 10^{-11}. \quad (1.5)$$

(iv) Hadronic light-by-light scattering contribution [16]:

$$a_\mu(\text{had. l-l}) = -52 (18) \times 10^{-11}, \quad (1.6)$$

and a similar result obtained independently in Ref. [17].

(v) Electroweak contribution of one [18] and two [19] loop orders:

$$a_\mu(\text{weak}) = 151 (4) \times 10^{-11}. \quad (1.7)$$

The current uncertainty in the theoretical value of  $a_\mu$  comes mostly from the hadronic contribution. It must be improved by at least a factor of two before we can extract useful physical information from the new high precision measurement and impose strong constraints on various candidates for possible extension of the standard model.

The hadronic contribution appears for the first time in the order  $\alpha^2$  as the effect of hadronic vacuum polarization. (See Fig. 1 of Ref. [9] for the Feynman graphs responsible for such a contribution.) Fortunately, the contribution of this type does not require explicit *ab initio* calculation based on QCD, since it is precisely calculable from the measured hadron production cross section in  $e^+e^-$  collisions [9–11]. Future measurements at VEPP-2M, VEPP-4M, DAΦNE and BEPS, as well as analysis of the hadronic tau decay data are expected to reduce the uncertainty of this contribution to the level that satisfies our need [12,20].

The contribution of the hadronic light-by-light scattering subdiagram is much smaller but is potentially a source of more serious problem because it has been difficult to express it in terms of experimentally accessible observables. At present it depends entirely on theoretical consideration. This contribution has been estimated recently by two groups within the framework of chiral perturbation theory and the  $1/N_c$  expansion [16,17]. The leading

terms arise from three types of diagrams shown in Fig. 1: (a) pion-loop contribution, (b) pseudoscalar pole contribution, and (c) quark-loop contribution. The results obtained in Ref. [16] for these diagrams are

$$\begin{aligned}
a_\mu(a)|_{\text{HKS}} &= -4.5 (8.1) \times 10^{-11}, \\
a_\mu(b)|_{\text{HKS}} &= -57.5 (11.4) \times 10^{-11}, \\
a_\mu(c)|_{\text{HKS}} &= 9.7 (11.1) \times 10^{-11}.
\end{aligned}
\tag{1.8}$$

They add up to (1.6). A small axial-vector contribution

$$a_\mu(\text{axial-vector})|_{\text{HKS}} = -1.74 \times 10^{-11}, \tag{1.9}$$

was also obtained but not included in (1.6). (See eq. (4.32) of Ref. [16].) The corresponding results obtained in [17] were

$$\begin{aligned}
a_\mu(a)|_{\text{BPP}} &= -19 (13) \times 10^{-11}, \\
a_\mu(b)|_{\text{BPP}} &= -85 (13) \times 10^{-11}, \\
a_\mu(c)|_{\text{BPP}} &= 21 (3) \times 10^{-11}.
\end{aligned}
\tag{1.10}$$

The effects of axial-vector and scalar poles were also considered in Ref. [17]:

$$\begin{aligned}
a_\mu(\text{axial-vector})|_{\text{BPP}} &= -2.5 (1.0) \times 10^{-11}, \\
a_\mu(\text{scalar})|_{\text{BPP}} &= -6.8 (2.0) \times 10^{-11}.
\end{aligned}
\tag{1.11}$$

Summing up (1.10) and (1.11), they obtained

$$a_\mu(\text{had. l-l})|_{\text{BPP}} = -92 (32) \times 10^{-11}. \tag{1.12}$$

The reasons for the difference between (1.8) and (1.10) are as follows: For the pion-loop contribution  $a_\mu(a)$  it is due to the fact that the effective Lagrangian responsible for (1.10) has a non-derivative  $\rho^0 \rho^0 \pi^+ \pi^-$  coupling while the corresponding term is absent in (1.8), which is obtained from a vector meson dominance (VMD) model with hidden local symmetry [21].

The absence of this term in the latter is a direct consequence of the fact that it satisfies the Ward-Takahashi identity [16] and a soft pion theorem for  $V^0\pi$  scattering amplitude [22].

In Ref. [17] an effective chiral Lagrangian was proposed which reproduces the earlier VMD result of Ref. [9] in terms of an interaction term consisting of an infinite series of derivatives of the pseudoscalar meson. These higher derivative terms are accompanied by a mass scale  $M_C$ , which, after their resummation, becomes just a pole mass corresponding to a vectorial degree of freedom. Their result will be justified if that  $M_C$  can be identified with the vector meson mass  $M_\rho$ . However, the analysis of the low energy behavior of the  $\rho^0\pi^+$  scattering prevents us from interpreting the above degree of freedom as being associated with the physical vector meson [22]. The scale  $M_C$  will have to be associated with another physical degree of freedom, which is heavier than  $M_\rho$ . For such an  $M_C$  the magnitude of the charged pion loop contribution based on their model will become smaller than that given in [17]. In this model the relation between the scale  $M_C$  and the resulting value of the charged pion loop contribution  $a_\mu(a)|_{\text{BPP}}$  in (1.10) is not transparent. For this reason we will henceforth choose  $a_\mu(a)|_{\text{HKS}}$  of (1.8) as the contribution of Fig. 1 (a).

The difference in the evaluation of  $a_\mu(b)$  is mainly due to the fact that only the contributions of the  $\pi^0$  pole and  $\eta$  pole are taken into account in (1.8) whereas (1.10) includes also the contribution of  $\eta'$ , which turned out to be not negligible [17]. When the  $\eta'$  contribution is added to (1.8) (see Sec. IV), the remaining difference for  $a_\mu(b)$  is no longer large and reflects mainly the ambiguity and difficulty in carrying out the chiral perturbation theory estimate beyond the momentum range of several hundred MeV.

Similarly, the difference between  $a_\mu(c)$  of (1.8) and (1.10) originates from the difficulty in estimating the contribution from large momentum region.

As is seen from (1.8) and (1.10), the most important contribution comes from the diagrams of type (b) in which neutral pseudoscalar mesons  $P$  ( $P = \pi^0, \eta$  and  $\eta'$ ) propagate between two  $P\gamma\gamma$  vertices, as shown in Fig. 2. As is well known, the chiral anomaly for  $\pi_0$ , for instance, can be expressed by the effective interaction

$$\mathcal{L} = -\frac{\alpha}{8\pi f_\pi} \pi^0 \epsilon^{\mu\nu\lambda\sigma} F_{\mu\nu} F_{\lambda\sigma}, \quad (1.13)$$

where  $f_\pi \simeq 93$  MeV is the pion decay constant, in the lowest order of chiral expansion. When applied to the calculation of  $a_\mu(b)$ , however, this Lagrangian leads to an ultraviolet-divergent result. This divergence arises from the triangular photon-photon-muon loop which is obtained by reducing the  $\pi^0\gamma\gamma$  vertex, represented by a large shaded blob on the left-hand side of Fig. 2(a), to a point. (Fig. 2(b) is convergent in the same limit.) It is a signal that the local interaction (1.13) is not applicable to photons and pions far off mass shell. In fact, such a triangular diagram will have a damping behavior in the underlying QCD theory, which protects its contribution to the muon  $g - 2$  from diverging.

In Ref. [16], four models were considered to examine the effect of various assumptions on the off-shell behavior of the  $\pi^0\gamma\gamma$  form factor:

- ( $b_1$ ) vector meson dominance (VMD) model, <sup>2</sup>
- ( $b_2$ ) quark triangular loop (QTL) model,
- ( $b_3$ ) QTL model combined with the VMD model,
- ( $b_4$ ) extended Nambu-Jona-Lasinio (ENJL) model [23].

The contribution  $a_\mu(b; \pi^0)$  of Fig. 2 evaluated by these models, and given by Eqs. (4.1), (4.3) and (4.4), and Table V (with  $g_A = 0.5$ ,  $M_C = 1$  GeV) of Ref. [16], are reproduced here:

$$\begin{aligned} a_\mu(b_1; \pi^0) &= -55.60 \times 10^{-11}, \\ a_\mu(b_2; \pi^0) &= -86.90 \times 10^{-11}, \\ a_\mu(b_3; \pi^0) &= -33.76 \times 10^{-11}, \\ a_\mu(b_4; \pi^0) &= -42.84 \times 10^{-11}. \end{aligned} \quad (1.14)$$

Similar calculations were carried out in Ref. [16] for the  $\eta$  resonance, too. The final value of  $a_\mu(b)$  reported in Ref. [16] and quoted in (1.8) is based mainly on the model ( $b_4$ ).

---

<sup>2</sup>The VMD model can be justified within the hidden local symmetry picture of the chiral model [21].

After completion of these calculations an experimental measurement of the  $P\gamma\gamma^*$  form factor, where  $P$  stands for  $\pi^0$ ,  $\eta$  or  $\eta'$ , came to our attention [24–26]. This is very important in the sense that it opens up the possibility of evaluating  $a_\mu(b)$  utilizing the experimental information instead of relying solely on theoretical consideration. This may enable us to reduce significantly the uncertainty in the evaluation of  $a_\mu(b)$ .

The purpose of this paper is to amplify the preliminary discussion in Ref. [16] about the implication of the measurements and discuss in full the effect of the measured  $P\gamma\gamma^*$  form factor (Sec. III) and possible impacts of the yet-to-be-measured  $P\gamma^*\gamma^*$  form factor on the evaluation of  $a_\mu(b)$  (Sec. IV). Before going into these sections, we review the theoretical aspects of the asymptotic behavior of the form factor of our interest in Sec. II. The last section (Sec. V) will be devoted to the summary and discussion of our results.

## II. THEORETICAL OFF-SHELL $\pi^0\gamma^*\gamma^*$ FORM FACTOR

Let us write the invariant  $P\gamma^*\gamma^*$  amplitude as

$$\begin{aligned} \mathcal{M}(\gamma^*(p_1, \lambda_1)\gamma^*(p_2, \lambda_2) \rightarrow P(q)) \\ = \epsilon_{\lambda_1}^\mu(p_1)\epsilon_{\lambda_2}^\nu(p_2)\epsilon_{\mu\nu\alpha\beta}p_1^\alpha p_2^\beta M_P(p_1^2, p_2^2, q^2 = m_P^2), \end{aligned} \quad (2.1)$$

and define the form factor  $F_P(p_1^2, p_2^2, q^2)$  by

$$F_P(p_1^2, p_2^2, q^2) = \frac{\pi f_P}{\alpha} M_P(p_1^2, p_2^2, q^2). \quad (2.2)$$

In the chiral limit ( $q^2 = m_P^2 = 0$ ), this is normalized as

$$F_P(0, 0, 0) = 1. \quad (2.3)$$

Let us first examine the off-shell behavior of the  $\pi^0\gamma^*\gamma^*$  form factor in the quark triangular loop (QTL) model. In this model, we find (ignoring isospin violation)

$$\begin{aligned} F_{\pi^0}^{\text{QTL}}(p_1^2, p_2^2, q^2) &= I_{m_u^2}(p_1^2, p_2^2, q^2) \\ &\equiv \int [dz] \frac{2m_u^2}{m_u^2 - z_2 z_3 p_1^2 - z_3 z_1 p_2^2 - z_1 z_2 q^2}, \end{aligned} \quad (2.4)$$

where  $[dz] = dz_1 dz_2 dz_3 \delta(1 - z_1 - z_2 - z_3)$ , and  $m_u \sim 300$  MeV is the constituent mass of up (and down) quark [27]. For  $p_1^2 = p_2^2 = q^2 = 0$  this function reduces to (2.3). Carrying out the integration one can readily find that

$$F_{\pi^0}^{\text{QTL}}(p_1^2, p_2^2, 0) = -\frac{m^2}{p_1^2 - p_2^2} \left[ \left\{ \ln \left( \frac{\sqrt{4m_u^2 - p_1^2} + \sqrt{-p_1^2}}{\sqrt{4m_u^2 - p_1^2} - \sqrt{-p_1^2}} \right) \right\}^2 - \left\{ \ln \left( \frac{\sqrt{4m_u^2 - p_2^2} + \sqrt{-p_2^2}}{\sqrt{4m_u^2 - p_2^2} - \sqrt{-p_2^2}} \right) \right\}^2 \right]. \quad (2.5)$$

For large  $p_1^2$  with  $p_2^2 = 0$  and  $q^2 = 0$  this has the asymptotic behavior of the form

$$F_{\pi^0}^{\text{QTL}}(p_1^2, 0, 0) \sim \frac{m_u^2}{-p_1^2} \left\{ \ln \left( \frac{-p_1^2}{m_u^2} \right) \right\}^2. \quad (2.6)$$

For large  $p_1^2 \sim p_2^2$  and  $q^2 = 0$  we find

$$F_{\pi^0}^{\text{QTL}}(p_1^2, p_1^2, 0) \sim \frac{2m_u^2}{-p_1^2} \ln \left( \frac{-p_1^2}{m_u^2} \right). \quad (2.7)$$

Note that both (2.6) and (2.7) have the same power behavior at large momentum transfer, differing only in the logarithmic factor.

Let us define the function  $\mathcal{F}_{\pi^0}$  by

$$\begin{aligned} \mathcal{F}_{\pi^0}(Q^2) &= \frac{1}{4\pi\alpha} |M_{\pi^0}(-Q^2, 0, 0)| \\ &= \frac{1}{4\pi^2 f_\pi} |F_{\pi^0}(-Q^2, 0, 0)|. \end{aligned} \quad (2.8)$$

Fig. 3 shows the momentum dependence of  $Q^2 \mathcal{F}_{\pi^0}(Q^2)$  for the cases  $(b_1)$ ,  $(b_2)$  and  $(b_3)$  together with the experimental data reported by CLEO collaboration [26]. This shows that the VMD model  $(b_1)$  fits the experimental data particularly well. The model  $(b_2)$  gives slower damping for higher momenta. This is because of the extra  $(\ln(-p_1^2))^2$  factor found in (2.6) which compensates for the leading damping  $1/p_1^2$  to some extent. The model  $(b_3)$ , on the other hand, predicts rapid decrease due to the stronger damping factor  $(\ln(-p_1^2))^2/p_1^4$ .

Nonperturbative analysis of asymptotic behavior of the exact form factor  $F_{\pi^0}(p_1^2, p_2^2, q^2)$  has also been carried out by several methods [27–29]. Various corrections to the result of [28] have also been considered: Ref. [30] discusses the effect of the parton transverse momentum.



Ref. [31] considers the gluonic radiative corrections to [30]. Ref. [32] derived an asymptotic formula applying the QCD sum rule [33]. These corrections have been compared with the data in [26]. Here, we concentrate on the methods of Refs. [27–29] since they are more directly related to the consideration of this paper.

For  $p_2^2 = q^2 = 0$  all three methods [27–29] predict the same leading power of momentum for large  $p_1^2$ . But the coefficients found are different:

$$\lim_{-p_1^2 \rightarrow \infty} F_{\pi^0}(p_1^2, 0, 0) = \frac{3}{N_c} \frac{2\pi^2 f_\pi^2}{-p_1^2}, \quad [28] \quad (2.9)$$

$$= \frac{2}{N_c} \frac{2\pi^2 f_\pi^2}{-p_1^2}, \quad [27] \quad (2.10)$$

$$= \frac{1}{N_c} \frac{2\pi^2 f_\pi^2}{-p_1^2}. \quad [29] \quad (2.11)$$

The asymptotic behavior of  $F_{\pi^0}(p_1^2, p_2^2, 0)$  for large  $p_1^2 = p_2^2$  has also been studied nonperturbatively [34]:

$$\lim_{-p_1^2 \rightarrow \infty} F_{\pi^0}(p_1^2, p_1^2, 0) = \frac{1}{N_c} \frac{2\pi^2 f_\pi^2}{-p_1^2}. \quad (2.12)$$

Ref. [29] states in addition that (2.11) holds for all values of  $p_2^2$  including  $p_2^2 \sim p_1^2$ .

Different asymptotic behaviors of (2.9), (2.10) and (2.11) presumably reflect different physical assumptions. Eq. (2.9) is obtained by appealing to the parton picture in the infinite momentum frame. The leading momentum power dependence there comes from the scaling behavior of the pion wave function. However the coefficient depends on the long distance aspect of the pion, which is vulnerable to theoretical prejudices. According to literatures [26,30,31] the ansatz adopted by Brodsky and Lepage for the pion wave function is not badly in conflict with the experiment.

Eq. (2.10) was obtained using the operator product expansion (OPE) technique, within the approximation of the dominance of operators of lowest dimension and twist [27]. The reliability of OPE and truncation of operators depend on the detailed prescription of how the large momentum limit is taken. In its application to the current issue the form factor is expanded in  $Q^2 = -(p_1 + p_2)^2/4$  and  $\omega = (p_1^2 - p_2^2)/Q^2$ . The leading power and its coefficient

can be determined including long distance effect only when the absolute magnitude of  $\omega$  is small. This is the case for large  $p_1^2 \sim p_2^2$  but not for large  $p_1^2$  with  $p_2^2$  fixed to 0. In the latter case the estimate based on the OPE is not trustworthy since  $\omega$  will not be restricted to small values and the long distance contributions associated with higher power of  $\omega$  might become as significant as the leading term [27].

The derivation of (2.11) relies on the Bjorken-Johnson-Low theorem [35]. This theorem is usually used to *define* the commutator of operators by postulating an appropriate asymptotic behavior for some correlation function. The asymptotic behavior in (2.11), on the other hand, is derived from the Bjorken-Johnson-Low (BJL) limit of the matrix element of the commutator of the electromagnetic currents [29]. The use of equal-time commutation relation of the quark fields turns this commutator into the axial current. This enabled them to express the relevant matrix element in terms of the pion decay constant  $f_\pi$ . However, this approach may not be reliable because the canonical equal-time commutation relation does not necessarily lead to the correct anomaly relation [36]. Whether this caution is also relevant for the evaluation of the commutator of the electromagnetic currents or not will not be pursued here. Irrespective of the validity of derivation of (2.11) in [29], we note that the asymptotic behavior of  $\pi^0\gamma\gamma^*$  in the time-like region will differ significantly from that measured in the space-like region. At present we cannot find reason to support the possibility that such a non-trivial continuation occurs between the two regions.

In order to compare the theoretical predictions of the  $\pi^0\gamma\gamma^*$  form factor with experiment, it is necessary to interpolate them from the asymptotic region to  $p_1^2 = 0$ , where they are fixed by the anomaly condition. Ref. [28] proposed a one-parameter interpolation formula

$$\mathcal{F}_{\pi^0}(Q^2) = \frac{1}{4\pi^2 f_\pi} \frac{1}{1 + Q^2/(8\pi^2 f_\pi^2)}, \quad (2.13)$$

where  $Q^2 = -p_1^2$ . The formula (2.13) has the same  $Q^2$  dependence as (3.1) if we choose  $8\pi^2 f_\pi^2 = M^2$ . Thus this interpolation reproduces the  $Q^2$  dependence very well. However, this also fixes the value of  $\mathcal{F}_{\pi^0}(0)$  which differs from the observed value by a factor of  $\sim 1.2$ . In this sense (2.13) does not fully reproduce the experimental data. Interpolations of (2.10)

and (2.11) will be even more difficult in this respect.

### III. $P\gamma\gamma^*$ FORM FACTOR

#### A. Experimental results

Depicted in Fig. 4 are the function  $Q^2\mathcal{F}_{\pi^0}(Q^2)$ , corresponding to the asymptotic form factors (2.9), (2.10) and (2.11), and the interpolation function (2.13), together with the observed  $\pi^0\gamma\gamma^*$  form factor provided by the recent CLEO data [26]. It is seen that none of the asymptotic behaviors shown there is fully consistent with the new data provided by CLEO for  $f_\pi = 93$  MeV.

On the other hand, it was noted [25] that the experimental data can be represented very well by the empirical formula

$$\mathcal{F}_{\pi^0}(Q^2) = \sqrt{\frac{64\pi\Gamma(\pi^0 \rightarrow \gamma\gamma)}{(4\pi\alpha)^2 m_{\pi^0}^3} \frac{1}{1 + (Q^2/\Lambda_{\pi^0}^2)}}, \quad (3.1)$$

if one chooses  $\Lambda_{\pi^0} \simeq 0.77$  GeV and  $\Gamma(\pi^0 \rightarrow \gamma\gamma) = 7.78$  (56) eV. The uncertainty in  $\Gamma$  is about  $\pm 7\%$  [37]. Note that this  $\Lambda_{\pi^0}$  is nearly identical with the physical  $\rho$  mass.

Similarly, the experimental data for the  $\eta$  and  $\eta'$  form factors can be represented well by

$$\mathcal{F}_P(Q^2) = \sqrt{\frac{64\pi\Gamma(P \rightarrow \gamma\gamma)}{(4\pi\alpha)^2 m_P^3} \frac{1}{1 + (Q^2/\Lambda_P^2)}}, \quad (3.2)$$

for  $P = \eta$  and  $\eta'$ , with the choice of  $\Lambda_\eta \simeq 0.77$  GeV and  $\Lambda_{\eta'} \simeq 0.85$  GeV. Here, to take account of non-zero mass of meson properly, we have modified (2.8) as

$$\mathcal{F}_P(Q^2) = \frac{1}{4\pi\alpha} \left| M_P(-Q^2, 0, m_P^2) \right|. \quad (3.3)$$

The life-times chosen are  $\Gamma(\eta \rightarrow \gamma\gamma) = 0.46$  (4) keV, and  $\Gamma(\eta' \rightarrow \gamma\gamma) = 4.26$  (19) keV. [37]

#### B. Effect of the $P\gamma\gamma^*$ form factor on muon $g - 2$

Let us now evaluate the pseudoscalar pole contribution to the muon  $g - 2$ , assuming that all virtual photons are modified by the  $P\gamma^*\gamma^*$  form factor in accord with the VMD

model. We consider two models. The first model ( $\text{VMD}_A$ ) assumes that the vector meson dominance is realized in terms of the  $\rho$  and  $\phi$  mesons of the form

$$M_P(p_1^2, p_2^2, q^2) = \frac{1}{f_P} \frac{\alpha}{\pi} \left\{ F_\rho^{\text{VMD}}(p_1^2, p_2^2, q^2) + \kappa_\phi(P) F_\phi^{\text{VMD}}(p_1^2, p_2^2, q^2) \right\}, \quad (3.4)$$

with

$$F_V^{\text{VMD}}(p_1^2, p_2^2, q^2) = \frac{M_V^2}{M_V^2 - p_1^2} \frac{M_V^2}{M_V^2 - p_2^2}, \quad (3.5)$$

for  $V = \rho$  and  $\phi$ , while  $\kappa_\phi(P)$  is treated as an adjustable parameter. Here we have adopted the approximation  $M_\rho \simeq M_\omega$ . Note that  $f_P$  appearing in (3.4) is not the usual decay constant. Rather it should be regarded as an ‘‘effective’’ decay constant. When we fit (3.4) with the experimental data we use the expression

$$\mathcal{F}_{\pi^0}(Q^2) = \sqrt{\frac{64\pi \Gamma(P \rightarrow \gamma\gamma)}{(4\pi\alpha)^2 m_P^3}} \times \frac{|M_P(-Q^2, 0, m_P^2)|}{|M_P(0, 0, m_P^2)|}, \quad (3.6)$$

which follows from (3.3) and

$$\Gamma(P \rightarrow \gamma\gamma) = \frac{m_P^3}{64\pi} |M_P(0, 0, m_P^2)|^2. \quad (3.7)$$

Note that fitting of (3.4) with data does not involve  $f_P$ . The value of  $f_P$  itself will be determined once we fix  $\kappa_\phi(P)$  from the experiment for a given  $\Gamma(P \rightarrow \gamma\gamma)$  through the relation

$$\begin{aligned} \Gamma(P \rightarrow \gamma\gamma) &= \frac{m_P^3}{64\pi} |M_P(0, 0, m_P^2)|^2 \\ &= \frac{1}{f_P^2} \frac{m_P^3}{64\pi} \left( \frac{\alpha}{\pi} \right)^2 \left| F_\rho^{\text{VMD}}(0, 0, m_P^2) + \kappa_\phi(P) F_\phi^{\text{VMD}}(0, 0, m_P^2) \right|^2. \end{aligned} \quad (3.8)$$

The second model ( $\text{VMD}_B$ ) assumes that the vector meson dominance is realized in terms of the experimental pole mass  $\Lambda_P$  obtained in [25]. We vary  $\Lambda_P$  within its error bars.

In the model  $\text{VMD}_A$  (or  $\text{VMD}_B$ ) the parameter  $\kappa_\phi(P)$  (or  $\Lambda_P$ ) is determined by fitting to the experimental data [26] for each pseudoscalar meson  $P$  and a fixed value of  $\Gamma(P \rightarrow \gamma\gamma)$  using the CERN library routine MINUIT. Here the confidence level of  $1\sigma$  is imposed to extract the uncertainty associated with the parameter  $\kappa_\phi(P)$  or  $\Lambda_P$ . We then examine the

effect of pseudoscalar poles on the muon anomaly based on this confidence level and the values of  $\Gamma(P \rightarrow \gamma\gamma)$  given in [37].

The results of our calculation are summarized in Tables I–VI. They have all been obtained by the integration routine VEGAS with 800 thousands sampling points per iteration and iterated 15 times. From the explicit calculation, the dependence on  $\Gamma(P \rightarrow \gamma\gamma)$  and  $\kappa_\phi(P)$  (or  $\Lambda_P$ ) is found to be rather simple, as can be partly inferred from those tables. To obtain the most likely value and the error of  $a_\mu(P)$  we follow the procedure described below for the  $\text{VMD}_A$  model. First we take the average of  $a_\mu(P)$  for  $(\Gamma(P \rightarrow \gamma\gamma)_{\text{max}}, \kappa_\phi(P)_{\text{center}})$  and that for  $(\Gamma(P \rightarrow \gamma\gamma)_{\text{min}}, \kappa_\phi(P)_{\text{center}})$  and deduce the errors associated with  $\Gamma(P \rightarrow \gamma\gamma)$  as the maximally allowed deviation from their mean value. Likewise the uncertainty associated with  $\kappa_\phi(P)$  can be found from  $a_\mu(P)$  for  $(\Gamma(P \rightarrow \gamma\gamma)_{\text{center}}, \kappa_\phi(P)_{\text{max}})$  and that for  $(\Gamma(P \rightarrow \gamma\gamma)_{\text{center}}, \kappa_\phi(P)_{\text{min}})$ . The central value of  $a_\mu(P)$  is set equal to the mean value of the above two averages. The total uncertainty is obtained by taking the square root of the sum of the squares of the two errors, assuming that the errors associated with  $\Gamma(P \rightarrow \gamma\gamma)$  and  $\kappa_\phi(P)$  are independently distributed. The same procedure also applies to the  $\text{VMD}_B$  model with  $(\Gamma(P \rightarrow \gamma\gamma), \Lambda(P))$  instead of  $(\Gamma(P \rightarrow \gamma\gamma), \kappa_\phi(P))$ .

From the results listed in Tables I–III we find that the contributions to the muon anomaly from  $\pi^0$ ,  $\eta^0$  and  $\eta'$  propagation in the  $\text{VMD}_A$  model are given by

$$\begin{aligned}
a_\mu(\pi^0, \text{VMD}_A) &= -0.045\ 8\ (29) \times \left(\frac{\alpha}{\pi}\right)^3, \\
a_\mu(\eta, \text{VMD}_A) &= -0.010\ 6\ (9) \times \left(\frac{\alpha}{\pi}\right)^3, \\
a_\mu(\eta', \text{VMD}_A) &= -0.009\ 4\ (7) \times \left(\frac{\alpha}{\pi}\right)^3.
\end{aligned} \tag{3.9}$$

For the  $\text{VMD}_B$  model we find similarly

$$\begin{aligned}
a_\mu(\pi^0, \text{VMD}_B) &= -0.045\ 8\ (29) \times \left(\frac{\alpha}{\pi}\right)^3, \\
a_\mu(\eta, \text{VMD}_B) &= -0.010\ 7\ (8) \times \left(\frac{\alpha}{\pi}\right)^3, \\
a_\mu(\eta', \text{VMD}_B) &= -0.009\ 5\ (7) \times \left(\frac{\alpha}{\pi}\right)^3.
\end{aligned} \tag{3.10}$$

The total contribution to muon  $g - 2$  from the pseudoscalar pole effect becomes

$$\begin{aligned} a_\mu(b, \text{VMD}_A) &= -0.065\ 8\ (32) \times \left(\frac{\alpha}{\pi}\right)^3 \\ &= -82.5\ (4.1) \times 10^{-11}, \end{aligned} \tag{3.11}$$

and

$$\begin{aligned} a_\mu(b, \text{VMD}_B) &= -0.066\ 0\ (31) \times \left(\frac{\alpha}{\pi}\right)^3 \\ &= -82.7\ (3.9) \times 10^{-11}, \end{aligned} \tag{3.12}$$

where the errors above were deduced assuming that the uncertainties associated with distinct mesons are normally distributed. These results are rather insensitive to the difference between the two models, both of which are already strongly constrained by the experiment.

Let us comment here on the pion decay constant. Note that every postulated form factor used in the previous analysis is proportional to  $1/f_P$  implementing the PCAC. Thus the contribution to  $a_\mu$  from each pseudoscalar meson propagation becomes proportional to  $1/f_P^2$ . In the previous analysis [9,16],  $f_\pi = 93\ \text{MeV}$  was used. This is the decay constant of the charged pion. That of the neutral pion is quoted as  $f_{\pi^0} \sim 84\ (3)\ \text{MeV}$  in [37]. Correspondingly the values of  $a_\mu$  predicted by all the above form factors receive the enhancement factor 1.22 if the latter value is used. But this implies that too much isospin breaking (about 10 %) shows up in the pion decay constants resulting from the mass difference of up and down quarks and electromagnetic corrections. Those values found in Refs. [24,25] for  $\pi^0$  were extracted from the use of pole-type form factor (3.1) corresponding to the VMD picture together with  $\Lambda_{\pi^0}^2 = 8\pi^2 f_{\pi^0}^2$ . This relation must not be trusted once we treat  $\Gamma(P \rightarrow \gamma\gamma)$  and  $\Lambda_P$  as two independent parameters. Its application might lead to a fictitiously large isospin violation in the pion decay constant. In our analysis throughout this paper, the decay constants are not the direct input, because its determination primarily depend on the form factor assumed. Instead, we use the partial decay width  $\Gamma(P \rightarrow \gamma\gamma)$  given in [37], and determine the effective decay constant according to an equation such as (3.8). This provides a phenomenological and totally self-contained algorithm.

#### IV. EFFECT OF THE $P\gamma^*\gamma^*$ FORM FACTOR ON MUON $g - 2$

For a full evaluation of the muon anomaly  $a_\mu(b)$ , we need information on the form factor for all values of  $p_1$  and  $p_2$ . In other words, we need information not only for large  $p_1^2$  with  $p_2^2 = 0$  or large  $p_2^2$  with  $p_1^2 = 0$  but also for the case where both  $p_1^2$  and  $p_2^2$  are large simultaneously. In the VMD model ( $b_1$ ) the off-shell  $\pi^0\gamma^*\gamma^*$  form factor for large  $p_1^2$  and  $p_2^2$  takes the form

$$F_{\pi^0}(p_1^2, p_2^2, 0) \propto \frac{1}{p^4} \quad \text{for} \quad p_1^2, p_2^2 \simeq p^2. \quad (4.1)$$

On the other hand the QTL model ( $b_2$ ) or a nonperturbative estimate shows much slower behavior ( $\sim 1/p^2$ ) as is seen from (2.7) and (2.12).

This suggests that the  $\pi^0\gamma^*\gamma^*$  form factor may have hard components for large  $p_1^2$  and  $p_2^2$ . Taking the asymptotic form (2.12) into account, we may, for instance, choose the function

$$F_{M_X}^{\text{LN}}(p_1^2, p_2^2) = \frac{1}{2} \left( \frac{M_X^2}{M_X^2 - p_1^2} + \frac{M_X^2}{M_X^2 - p_2^2} \right), \quad (4.2)$$

as a candidate of the hard component. Another possibility is to use (2.7) itself. With this in mind we consider two models:

- (I) Linear combination of the  $\text{VMD}_A$  model and the function (4.2),
- (II) Linear combination of the  $\text{VMD}_A$  model and the QTL model ( $b_2$ ).

We will not discuss the  $\text{VMD}_B$  model since the difference between the  $\text{VMD}_B$  model and  $\text{VMD}_A$  model is small. Let us introduce a parameter  $\beta_P$  to describe the deviation from the  $\text{VMD}_A$  model. The best value of  $\beta_P$  depends on the species  $P$  of pseudoscalar meson. To be more specific, we write the scalar part of the invariant amplitude (2.1) as

$$M_P(p_1^2, p_2^2, q^2) = \frac{1}{f_P} \frac{\alpha}{\pi} \left[ F_\rho^{\beta_P}(p_1^2, p_2^2, q^2) + \kappa_\phi(P) F_\phi^{\beta_P}(p_1^2, p_2^2, q^2) \right], \quad (4.3)$$

where, for the extended model (I),

$$F_V^{\beta_P}(p_1^2, p_2^2, q^2) = (1 - \beta_P) F_V^{\text{VMD}}(p_1^2, p_2^2) + \beta_P F_{M_X(P)}^{\text{LN}}(p_1^2, p_2^2), \quad (4.4)$$

and, for the extended model (II),

$$F_V^{\beta_P}(p_1^2, p_2^2, q^2) = (1 - \beta_P)F_V^{\text{VMD}}(p_1^2, p_2^2) + \beta_P F_V^{\text{QTL}}(p_1^2, p_2^2, q^2). \quad (4.5)$$

Here  $F_V^{\text{VMD}}(p_1^2, p_2^2)$  is the form factor (3.5) in  $\text{VMD}_A$  model,  $F_{M_X}^{\text{LN}}(p_1^2, p_2^2)$  is given by (4.2) in which  $M_X(P)$  is assumed, for simplicity, to take the same value for  $\rho$  and  $\phi$ , and

$$F_V^{\text{QTL}}(p_1^2, p_2^2, q^2) = \begin{cases} I_{m_u}(p_1^2, p_2^2, q^2) & \text{for } V = \rho, \\ I_{m_s}(p_1^2, p_2^2, q^2) & \text{for } V = \phi. \end{cases} \quad (4.6)$$

$I_{m_u}$  is defined in (2.4).  $I_{m_s}$  takes account of the fact that  $\phi$  meson is dominated by the  $s\bar{s}$  state. Again the ‘‘effective’’ decay constant  $f_P$  in (4.3) does not have the usual meaning and is determined in the same way as in Sec. III B. In the extended model (II), for instance, for each meson  $P$  and a given value of  $\Gamma(P \rightarrow \gamma\gamma)$ , the direct fit to the experimental data determines the parameters  $\beta_P$  and  $\kappa_\phi(P)$ , which give the least value of  $\chi^2$  according to (3.6). Once the values of  $\Gamma(P \rightarrow \gamma\gamma)$ ,  $\kappa_\phi(P)$  and  $\beta_P$  are fixed, a relation similar to (3.8) leads to  $f_P$ .

Note that the extended model (I) of (4.4) has an incorrect asymptotic behavior for finite  $p_1^2$  or  $p_2^2$ . Thus it must be regarded as an empirical formula designed to fit the experimental data and applicable only up to the largest momentum transfer of the experimental data. We use it nevertheless because of simplicity and because its effect on the muon  $g - 2$  is small as far as  $\beta_P$  is small. The extended model (II) is also not very satisfactory since the QTL part has a logarithmic growth which distorts the form factor even for moderately large momentum transfers. Thus both must be treated with some caution.

### A. Extended model (I)

The extended model (I) involves one additional parameter  $M_X$ , and the best fitting values of  $\kappa_\phi(P)$  and  $\beta_P$  change as  $M_X$  changes even for the same value of  $\Gamma(P \rightarrow \gamma\gamma)$ . To avoid time-consuming and excessive analysis, we first perform two parameter fitting for fixed  $M_X$  and  $\Gamma(P \rightarrow \gamma\gamma)$  to determine a set  $(\beta_P, \kappa_\phi(P))$  that gives the best  $\chi^2$ . Next we determine



the range of  $\kappa_\phi$  allowed at  $1\sigma$  confidence level with  $\beta_P$  fixed to the best value obtained above, and *vice versa*. The result of such a fitting is summarized in Tables VII–IX. They show that  $\beta_P$  is small in general and thus does not favor strong presence of hard component. Note that a large  $M_X$  implies near  $q$ -independence of the term:

$$\frac{M_X^2}{M_X^2 - q^2} \rightarrow 1 \quad \text{for } M_X^2 \rightarrow \infty \text{ with fixed } q^2. \quad (4.7)$$

This means that the formula (4.4) tends to a constant  $\beta_P$  and hence gives rise to a divergence of the muon  $g - 2$  proportional to  $\ln M_X$ . Larger  $M_X$  also leads to larger minimum of  $\chi^2$ . Thus we restrict  $M_X$  to the values below 6 GeV, and examine the effect of this term on the muon  $g - 2$ .

The computation of muon  $g - 2$  has been performed for several sets of  $(\beta, \kappa_\phi)$ , in which either  $\beta$  or  $\kappa_\phi$  is its best fitted value for given  $M_X$  and  $\Gamma(P \rightarrow \gamma\gamma)$ . The results listed in Tables X–XII for the extended model (I) have been obtained by integration with 800 thousands sampling points per iteration which is iterated 15 times. The errors generated by the numerical integration itself are not explicitly stated since they are all under 0.05 %, far below the errors arising from the uncertainty in  $\Gamma(P \rightarrow \gamma\gamma)$ .

Let us first focus our attention on the case  $M_X = M_\rho$  in Tables X–XII, which is the lowest value of the scale  $M_X$  characterizing the modification of the high energy behavior in the present model. To deal with these data we adopt the same procedure as in the case of the VMD model. For instance the uncertainty associated with the variation of  $\Gamma(P \rightarrow \gamma\gamma)$  can be read off from  $a_\mu(P)$  for  $(\Gamma(P \rightarrow \gamma\gamma)_{\max}, \beta(P)_{\text{center}}, \kappa_\phi(P)_{\text{center}})$  and that for  $(\Gamma(P \rightarrow \gamma\gamma)_{\min}, \beta(P)_{\text{center}}, \kappa_\phi(P)_{\text{center}})$ . The uncertainty associated with the variation of  $\beta(P)$  and  $\kappa_\phi(P)$  will be found similarly. We take the average of three tentative central values to obtain the central value of  $a_\mu(P)$  given below. The combined error is obtained by taking the square root of the sum of squares of the errors. The contributions to muon anomaly from  $\pi^0$ ,  $\eta^0$  and  $\eta'$  propagation in the extended model (I) can then be written as

$$a_\mu(\pi^0, \text{(I)}) = -0.045 \ 6 \ (28) \times \left(\frac{\alpha}{\pi}\right)^3,$$

$$\begin{aligned}
a_\mu(\eta, \text{I}) &= -0.010\ 3\ (9) \times \left(\frac{\alpha}{\pi}\right)^3, \\
a_\mu(\eta', \text{I}) &= -0.009\ 0\ (6) \times \left(\frac{\alpha}{\pi}\right)^3,
\end{aligned}
\tag{4.8}$$

where the uncertainties are estimated assuming that the error distribution associated with  $\Gamma(P \rightarrow \gamma\gamma)$ ,  $\beta_P$  and  $\kappa_\phi(P)$  are normal and independent. The result obtained assuming  $M_X = 2$  GeV is nearly identical with (4.8). The result for larger values of  $M_X$  deviates only slightly from (4.8), except for the considerable  $M_X$  dependence seen in  $a_\mu(\eta, \text{I})$ .

### B. Extended model (II)

The trial form factor for the extended model (II) is the  $\text{VMD}_A$  model augmented slightly by a QTL term. The additional term receives a strong constraint from the experimental data as is shown in Tables XIII–XV. This is anticipated because the logarithmic factor in (2.7) of the QTL model is quite visible even in the moderately large momentum region, and hence receives a strong constraint from experiment. Tables XVI–XVIII show the prediction for the muon  $g - 2$  from the trial form factor (4.5) for each pseudoscalar meson under the constraint of the parameters in Tables XIII–XV, in which all the results have been obtained by the integration with 500 thousands sampling points per iteration which is iterated 25 times. In the manner similar to that of Sec. IV A, the contributions to muon anomaly from  $\pi^0$ ,  $\eta^0$  and  $\eta'$  propagation in the extended model (II) are estimated to be

$$\begin{aligned}
a_\mu(\pi^0, \text{II}) &= -0.045\ 6\ (28) \times \left(\frac{\alpha}{\pi}\right)^3, \\
a_\mu(\eta, \text{II}) &= -0.006\ 4\ (9) \times \left(\frac{\alpha}{\pi}\right)^3, \\
a_\mu(\eta', \text{II}) &= -0.008\ 7\ (7) \times \left(\frac{\alpha}{\pi}\right)^3.
\end{aligned}
\tag{4.9}$$

It is seen that the QTL modification to the VMD results of Sec. III is larger compared with the case of extended model (I). In particular, the  $\eta$  contribution is reduced in magnitude compared to that obtained in the other scheme. Comparison of (4.9) with (4.8) shows that the additional term in case (II) leads to a better  $\chi^2$ . Moreover the signs of  $\kappa_\phi$  for  $\eta$  and

$\eta'$  tend to become negative in the present case compared to the  $\text{VMD}_A$  model, as can be seen from Tables II, III, XIV and XV. The opposite signs of  $\rho$  and  $\phi$  contributions result in the decrease of absolute magnitudes of  $\eta$  and  $\eta'$  contributions. This relative minus sign is required to fit to the experimental data once the form factor contains a QTL component which enhances the contribution of large momentum region. In the sense that this region is beyond control of the experimental data and the logarithmic enhancement may be an artifact of perturbation theory, however, the result (4.9) must be treated with some caution, and should be accorded less weight than the extended model (I).

Note that the flavor SU(3) relation implies  $\kappa_\phi(\eta) \simeq -0.28$  and  $\kappa_\phi(\eta') \simeq 0.29$  for  $\theta \simeq -10.1^\circ$  [37]. While the signs of  $\kappa_\phi(\eta)$  and  $\kappa_\phi(\eta')$  in the extended model (I) are consistent with the SU(3) relation, those in the extended model (II) are not. Of course this does not mean that one model is more appropriate than the other. In the first place, it is obscure whether SU(3) breaking effect due to strange quark mass is substantial or not. Secondly, we do not know the relevance of the  $U(1)_A$  anomaly (QCD anomaly) contribution to the  $\eta_0 \rightarrow \gamma\gamma$  ( $\eta_0$  is the SU(3) singlet component) vertex. These questions have been examined for  $P \rightarrow \gamma\gamma$  in [38], and for another decay channel in [39], in which the subtlety that the presence of QCD anomaly raises is explored in identifying the decay constant invariant under renormalization group, inducing a nonperturbative ambiguity associated with each decay channel. We shall not discuss its relevance quantitatively here. We believe that these effects can be incorporated in a few constants parametrizing the form factor we chose, by fitting to the observed pseudoscalar production cross section through the two photon process [24-26].

## V. SUMMARY AND DISCUSSION

In this paper we reexamined the pseudoscalar meson pole contributions to the muon  $g-2$  taking account of the measured  $P\gamma\gamma^*$  form factor and of possible effect of the postulated  $P\gamma^*\gamma^*$  form factor. Insofar as we demand that these form factors respect the measured

strength of  $P\gamma\gamma^*$  for large momentum ( $\sim$  several GeV) with one photon on the mass-shell, the form factor cannot deviate from the VMD model substantially.

The results (4.8) and (4.9) of the extended models have somewhat smaller overall uncertainties than the results (3.11) and (3.12) of the  $\text{VMD}_A$  and  $\text{VMD}_B$  models. This may be due to better flexibility of the extended models.

Inspection of (4.8) and (4.9) shows that the contribution of the  $\pi^0\gamma^*\gamma^*$  form factor is nearly identical for both models while the contribution of the  $\eta\gamma^*\gamma^*$  form factor shows considerable dependence on the assumed structure of hard component. This may not be surprising since the effect of hard component will be stronger for  $\eta$  than for  $\pi^0$ . Better agreement of the  $\eta'\gamma^*\gamma^*$  cases may just be a matter of coincidence. The  $\eta'$  contribution in (4.8) is somewhat smaller than that of  $\eta$ , in contrast to the results of the ENJL model and the extended model (II), both of which contain the QTL form factor at least partly.

Note that either (4.8) or (4.9) cannot be taken as our best estimate based on the experimental data only since they depend on theoretical assumption about the hard component. Instead they must be regarded as providing a measure of uncertainty in  $a_\mu$  due to the unknown effect of the  $P\gamma^*\gamma^*$  form factor. Our calculation shows that this uncertainty comes mainly from the contribution of  $\eta\gamma^*\gamma^*$  form factor. For the reasons discussed in Sec. IV B, we believe that  $a_\mu(\eta, \text{II})$  is less reliable than  $a_\mu(\eta, \text{I})$ . But their difference  $0.0039(\alpha/\pi)^3$  may be regarded as a measure of theoretical uncertainty.

Based on these considerations, we adopt (3.12) as our best estimate and choose as its uncertainty the statistical combination of the error in (3.12), which comes from the experimental uncertainty in the  $P\gamma\gamma^*$  measurement, and the effect described above due to possible presence of hard component in the  $P\gamma^*\gamma^*$  form factor. We thus arrive at the total pseudoscalar pole contribution

$$a_\mu(\pi + \eta + \eta') = -82.7 (6.4) \times 10^{-11}. \quad (5.1)$$

The uncertainty here has been reduced to one half of the previous result (1.8). That the result (1.10) from Ref. [17] is close to our result (5.1) is not surprising since the modified

ENJL model of [17] contains an adjustable free parameter. The crucial difference between the old results (1.8), (1.10) and the new result (5.1) is that the latter is much less dependent on the theoretical ambiguity, being determined by the experimental data to a large extent.

The theoretical uncertainty in (5.1) reflects the absence of data on the  $P\gamma^*\gamma^*$  form factor. It is useful to note, however, that it is possible to gain some insight for the effect of the  $P\gamma^*\gamma^*$  form factor based on the measurements of  $\pi^0 \rightarrow e^+e^-$  and  $\eta \rightarrow \mu^+\mu^-$  decays, both of which involve the  $P\gamma^*\gamma^*$  form factor. The measured branching ratios [40]

$$B_{\text{meas}}(\eta \rightarrow \mu^+\mu^-) \equiv \frac{\Gamma(\eta \rightarrow \mu^+\mu^-)}{\Gamma(\eta \rightarrow \gamma\gamma)} = 1.4 (0.2) \times 10^{-5}, \quad (5.2)$$

and

$$B_{\text{meas}}(\pi^0 \rightarrow e^+e^-) \equiv \frac{\Gamma(\pi^0 \rightarrow e^+e^-)}{\Gamma(\pi^0 \rightarrow \gamma\gamma)} = 7.3 (1.9) \times 10^{-8}, \quad (5.3)$$

where the latter is a weighted average of the data from Ref. [41] are in good agreement with the theoretical values based on the VMD model [42] <sup>3</sup>

$$\begin{aligned} B_{\text{VMD}}(\eta \rightarrow \mu^+\mu^-) &\equiv \frac{\Gamma(\eta \rightarrow \mu^+\mu^-)}{\Gamma(\eta \rightarrow \gamma\gamma)} = (1.14_{-0.03}^{+0.07}) \times 10^{-5}, \\ B_{\text{VMD}}(\pi^0 \rightarrow e^+e^-) &\equiv \frac{\Gamma(\pi^0 \rightarrow e^+e^-)}{\Gamma(\pi^0 \rightarrow \gamma\gamma)} = 6.41 (0.19) \times 10^{-8}. \end{aligned} \quad (5.4)$$

The differences between these values are presumably due to the effect of the  $P\gamma^*\gamma^*$  form factor. It appears to be no greater than 15 %. In principle, such an information can lead to a completely model-independent evaluation of the pseudoscalar pole contribution to the muon  $g - 2$ . Further improvement in these measurements will thus be of great interest.

Unlike the pseudoscalar pole contribution discussed in this paper, the other contributions of hadronic light-by-light scattering type from Fig. 1 remain vulnerable to various theoretical ambiguities. The axial-vector pole contribution (1.11) was obtained entirely based on the ENJL model, which is certainly not satisfactory in the sense that it does not lead to the correct asymptotic behavior for the  $\pi^0\gamma\gamma^*$  vertex [17]. Based on the estimates (1.9)

---

<sup>3</sup>We thank J. F. Donoghue for calling our attention to this reference.

and (1.11) the axial-vector pole contribution seems to be relatively minor compared with the effect (5.1) of the pseudoscalar pole propagation. Since nothing better is available at present and since it is very small, we choose (1.9) as our best estimate of the axial vector contribution assigning an uncertainty as large as the value (1.9) itself. The axial-vector meson contribution may be estimated more reliably if the off-shell structure of  $A\gamma\gamma$  vertex is available from the experiment as was the case for the  $P\gamma\gamma$  vertex.

Another possible pole effect, the scalar resonance inferred within the ENJL model, has not been observed convincingly. It may not be surprising if an "exact" QCD calculation leads only to a continuum spectrum instead of producing a broad resonance in the scalar channel of the corresponding energy scale (  $0.6 \lesssim \sqrt{s} \lesssim 1.5$  GeV ).

In the absence of any resonance in the low energy region (below several hundred MeV) in the  $\pi - \pi$  and  $q\bar{q}$  channels, the pion-loop contribution  $a_\mu(a)$  and the quark-loop contribution  $a_\mu(c)$  may be regarded as representing the effect of the continuum spectrum. Previous analysis [16,17] shows that  $a_\mu(a)$  and  $a_\mu(c)$  have sizable contributions from the region of higher momentum transfer where neither chiral perturbation theory nor the  $1/N_c$  expansion may provide reliable guidance. Even mutual independence of the three types of diagrams of Fig. 1 might not hold valid there. For lack of better argument, however, we choose the sum of  $a_\mu(a)$  and  $a_\mu(c)$  as a crude estimate of the entire continuum contribution. The scalar pole contribution may be regarded as included in this estimate.

Finally, collecting  $a_\mu(a)$  and  $a_\mu(c)$  from (1.8), the pseudoscalar meson pole contribution from (5.1), and including (1.9), we present

$$a_\mu(\text{had l-l}) = -79.2 (15.4) \times 10^{-11} \tag{5.5}$$

as our best estimate of the total hadronic light-by-light scattering contribution to the muon anomaly. Here the uncertainty is obtained from the errors of various components assuming normal distribution. If the uncertainties are combined additively, one would obtain  $\sim \pm 30 \times 10^{-11}$ .

Further progress in theory would have to wait for the lattice QCD calculation of the

hadronic four-point function. In view of the recent progress in the lattice QCD and rapidly increasing computing power, such a calculation may no longer be a far-fetched dream. As of now, the theoretical value of the muon  $g - 2$ , which consists of (1.3), (1.4), (1.5), (1.7), and our new analysis of the hadronic light-by-light scattering effect (5.5), is given by

$$a_\mu(\text{th}) = 116\,591\,687\,(96) \times 10^{-11}. \quad (5.6)$$

The largest source of theoretical uncertainty remains to be the hadronic vacuum polarization effect (1.4). Better measurements of this effect are urgently needed.

### ACKNOWLEDGMENTS

T. K. thanks the hospitality of KEK, High Energy Accelerator Research Organization, where part of this work was carried out. We thank V. Savinov for informing us of the up-dated result from CLEO and for useful discussions. Thanks are due to B. N. Taylor, P. J. Mohr, and B. L. Roberts for helpful comments. T. K.'s work is supported in part by the U. S. National Science Foundation. M. H. is a JSPS Fellow supported in part by the Grand-in-Aid for Scientific Research from the Ministry of Education, Science and Culture of Japan.

## REFERENCES

- [1] J. P. Miller *et al.*, AIP, Proceedings of the 6th Conference on the Intersections between Particle and Nuclear Physics (CIPANP), May 1997 (to be published).
- [2] J. Bailey *et al.*, Phys. Lett. **68B**, 191 (1977); F. J. M. Farley and E. Picasso, in *Quantum Electrodynamics*, edited by T. Kinoshita (World Scientific, Singapore, 1990), pp. 479 - 559.
- [3] J. Lopez, D. V. Nanopoulos and X. Wang, Phys. Rev. D **49**, 366 (1991); U. Chattopadhyay and P. Nath, Phys. Rev. D **53**, 1648 (1996); T. Moroi, Phys. Rev. D **53**, 6565 (1996); *ibid.* **56**, 4424(E) (1997); M. Carena, G. F. Giudice and C. E. M. Wagner, Phys. Lett. B **390**, 234 (1997).
- [4] ALEPH Collaboration, D. Buskulic *et al.*, Phys. Lett. B **373**, 246 (1996); OPAL Collaboration, G. Alexander *et al.*, Phys. Lett. B **377**, 181 (1996); L3 Collaboration, M. Acciarri *et al.*, Phys. Lett. B **377**, 289 (1996); DELPHI Collaboration, P. Abreu *et al.*, Phys. Lett. B **382**, 323 (1996).
- [5] G. Couture and H. König, Phys. Rev. D **53**, 555 (1996).
- [6] H1 Collaboration, C. Adloff *et al.*, Z. Phys. C **74**, 191 (1997); ZEUS Collaboration, J. Breitweg *et al.*, Z. Phys. C **74**, 207 (1997).
- [7] R. S. Van Dyck, Jr., P. B. Schwinberg and H. G. Dehmelt, Phys. Rev. Lett. **59**, 26 (1987).
- [8] T. Kinoshita, Rep. Prog. Phys. **59**, 1459 (1996).
- [9] T. Kinoshita, B. Nižić and Y. Okamoto, Phys. Rev. D **31**, 2108 (1985).
- [10] C. Bouchiat and L. Michel, J. Phys. Radium **22**, 121 (1961); L. Durand, Phys. Rev. **128**, 441 (1962).
- [11] J. A. Casas, C. López and F. J. Ynduráin, Phys. Rev. D **32**, 736 (1985); L. Martinovič



- and S. Dubnička, Phys. Rev. D **42**, 884 (1990); L. M. Kurdadze *et al.*, JETP Lett. **43**, 643 (1986); JETP Lett. **47**, 512 (1988); L. M. Barkov *et al.*, Sov. J. Nucl. Phys. **47**, 248 (1988); S. I. Dolinsky *et al.*, Phys. Rept. **C202**, 99 (1991); Phys. Lett. B **174**, 453 (1986); S. Eidelman and F. Jegerlehner, Z. Phys. **C67**, 585 (1995).
- [12] W. A. Worstell and D. H. Brown, Phys. Rev. D **54**, 3237 (1996).
- [13] R. Alemany, M. Davier and A. Höcker, Report No. hep-ph/9703220 (unpublished).
- [14] CLEO Collaboration, Report No. CLEO CONF 97-31, EPS97 368 (unpublished).
- [15] B. Krause, Phys. Lett. B **390**, 392 (1997).
- [16] M. Hayakawa, T. Kinoshita and A. I. Sanda, Phys. Rev. Lett. **75**, 790 (1995); Phys. Rev. D **54**, 3137 (1996).
- [17] J. Bijnens, E. Pallante and J. Prades, Phys. Rev. Lett. **75**, 1447 (1995); *ibid.* **75**, 3781 (1995); Nucl. Phys. **B474**, 379 (1996);
- [18] K. Fujikawa, B. W. Lee and A. I. Sanda, Phys. Rev. D **6**, 2923 (1972); R. Jackiw and S. Weinberg, Phys. Rev. D **5**, 2473 (1972); G. Altarelli, N. Cabibbo and L. Maiani, Phys. Lett. **40B**, 415 (1972); I. Bars and M. Yoshimura, Phys. Rev. D **6**, 374 (1972); W. A. Bardeen, R. Gastmans and B. E. Lautrup, Nucl. Phys. **B46**, 319 (1972).
- [19] A. Czarnecki, B. Krause and W. J. Marciano, Phys. Rev. Lett. **76**, 3267 (1996); Phys. Rev. D **52**, 2619 (1995); S. Peris, M. Perrottet and E. de Rafael, Phys. Lett. B **355**, 523 (1995); T. V. Kukhto, E. A. Kuraev, A. Schiller and Z. K. Silagadze, Nucl. Phys. **B371**, 567 (1992).
- [20] R. Barbieri and E. Remiddi, in “*Second DAΦNE Physics Handbook*”, edited by L. Maiani, L. Pancheri and N. Paver ( INFN, Franzini, 1995 ) Vol. II, p. 467; P. Franzini, *ibid*, p.471.
- [21] M. Bando, T. Kugo, and K. Yamawaki, Phys. Rept. **164**, 217 (1988).

- [22] M. Hayakawa, Phys. Rev. D **54**, 6586 (1996).
- [23] J. Bijnens, Phys. Rept. **265**, 369 (1996).
- [24] H.-J. Behrend *et al.* (CELLO Collaboration), Z. Phys. C**49**, 401 (1991).
- [25] D. M. Asner *et al.* (CLEO Collaboration), Report No. CLEO CONF95-24, EPS0188 (unpublished).
- [26] CLEO Collaboration, Report No. CLNS preprint 97/1477, hep-ex/9707031 (unpublished).
- [27] A. V. Manohar, Phys. Lett. B **244**, 101 (1990).
- [28] G. P. Lepage and S. J. Brodsky, Phys. Lett. B **87**, 359 (1979).
- [29] J.-M. Gérard and T. Lahna, Phys. Lett. B **356**, 381 (1995).
- [30] F.-G. Cao, T. Huang and B.-Q. Ma, Phys. Rev. D **53**, 6582 (1996); F.-G. Cao and T. Huang, Report No. BIHEP-TH-95-14, hep-ph/9612233 (unpublished).
- [31] R. Jacob, P. Kroll and M. Raulfs, J. Phys. G **22**, 45 (1996).
- [32] A. Radyushkin and R. Ruskov, Phys. Lett. **B374**, 173 (1996); Nucl. Phys. **B481**, 625 (1996); Report No. JLAB-THY-97-24, hep-ph/9706518 (unpublished).
- [33] M. A. Shifman, A. I. Vainshtein and V. I. Zakharov, Nucl. Phys. **B147**, 385 (1979).
- [34] V. A. Novikov, M. A. Shifman, A. I. Vainshtein, M. B. Voloshin and V. I. Zakharov, Nucl. Phys. **B237**, 525 (1984).
- [35] J. D. Bjorken, Phys. Rev. **148**, 1467 (1966); K. Johnson and F. E. Low, Suppl. Prog. Theor. Phys. **37, 38**, 74 (1966).
- [36] R. Jackiw and K. Johnson; Phys. Rev. **182**, 1459 (1969); S. Adler and D. G. Boulware, Phys. Rev. **184**, 1740 (1969); R. Christos, Phys. Rept. **116**, 251 (1984).

- [37] Particle Data Group: Review of Particle Properties, Phys. Rev. D **54**, 1 (1996).
- [38] G. M. Shore and G. Veneziano, Nucl. Phys. **B381**, 3 (1992).
- [39] R. Akhoury and J.-M. Frère, Phys. Lett. B **220**, 258 (1989); Riazuddin and R. E. Marshak, Prog. Theor. Phys. **91**, 151 (1994); P. Ball, J.-M. Frère and M. Tytgat, Phys. Lett. B **365**, 367 (1996); N. Evans, S. D. H. Hsu and M. Schwetz, Phys. Lett. B **382**, 138 (1996).
- [40] R. S. Kessler *et al.*, Phys. Rev. Lett. **70**, 892 (1993).
- [41] A. Deshpande *et al.*, Phys. Rev. Lett. **71**, 27 (1993); K. S. McFarland *et al.*, Phys. Rev. Lett. **71**, 31 (1993).
- [42] L. Ametller, A. Bramon and E. Massó, Phys. Rev. D **48**, 3388 (1993).

TABLES

TABLE I.  $\pi^0$  contribution to muon  $g - 2$  in the  $\text{VMD}_A$  model.

$\Gamma(\pi^0 \rightarrow \gamma\gamma)$ [eV]	$\kappa_\phi(\pi^0)$	$a_\mu(\pi^0)/(\alpha/\pi)^3$
7.22	-0.01	-0.041 87 (2)
7.22	0.12	-0.043 56 (2)
7.22	0.27	-0.045 28 (2)
7.78	-0.07	-0.044 03 (2)
7.78	0.04	-0.045 80 (2)
7.78	0.16	-0.047 54 (2)
8.34	-0.12	-0.046 17 (2)
8.34	-0.03	-0.047 95 (2)
8.34	0.08	-0.049 76 (2)

TABLE II.  $\eta$  contribution to muon  $g - 2$  in the  $\text{VMD}_A$  model.

$\Gamma(\eta \rightarrow \gamma\gamma)$ [keV]	$\kappa_\phi(\eta)$	$a_\mu(\eta)/(\alpha/\pi)^3$
0.42	0.04	-0.009 646 (4)
0.42	0.19	-0.010 235 (4)
0.42	0.38	-0.010 843 (4)
0.46	-0.04	-0.009 910 (4)
0.46	0.07	-0.010 726 (4)
0.46	0.22	-0.011 349 (4)
0.50	-0.10	-0.010 594 (4)
0.50	-0.01	-0.011 211 (4)
0.50	0.13	-0.011 921 (5)

TABLE III.  $\eta'$  contribution to muon  $g - 2$  in the  $\text{VMD}_A$  model.

$\Gamma(\eta' \rightarrow \gamma\gamma)$ [keV]	$\kappa_\phi(\eta')$	$a_\mu(\eta')/(\alpha/\pi)^3$
4.07	0.25	-0.008 584 (4)
4.07	0.48	-0.009 190 (4)
4.07	0.82	-0.009 818 (5)
4.26	0.19	-0.008 766 (4)
4.26	0.39	-0.009 380 (4)
4.26	0.67	-0.010 013 (5)
4.45	0.13	-0.008 947 (4)
4.45	0.31	-0.009 562 (4)
4.45	0.55	-0.010 205 (5)

TABLE IV.  $\pi^0$  contribution to muon  $g - 2$  in the  $\text{VMD}_B$  model.

$\Gamma(\pi^0 \rightarrow \gamma\gamma)$ [eV]	$\Lambda_{\pi^0}$ [GeV]	$a_\mu(\pi^0)/(\alpha/\pi)^3$
7.22	0.77	-0.041 86 (2)
7.22	0.80	-0.043 78 (2)
7.22	0.82	-0.045 67 (2)
7.78	0.75	-0.043 83 (2)
7.78	0.78	-0.045 85 (2)
7.78	0.80	-0.047 83 (2)
8.34	0.73	-0.045 75 (2)
8.34	0.76	-0.047 86 (2)
8.34	0.79	-0.049 93 (2)

TABLE V.  $\eta$  contribution to muon  $g - 2$  in the  $\text{VMD}_B$  model.

$\Gamma(\eta \rightarrow \gamma\gamma)$ [keV]	$\Lambda_\eta$ [GeV]	$a_\mu(\eta)/(\alpha/\pi)^3$
0.42	0.78	-0.009 645 (4)
0.42	0.81	-0.010 291 (4)
0.42	0.84	-0.010 940 (4)
0.46	0.76	-0.010 066 (4)
0.46	0.79	-0.010 742 (4)
0.46	0.81	-0.011 419 (5)
0.50	0.74	-0.010 467 (4)
0.50	0.77	-0.011 171 (4)
0.50	0.79	-0.011 876 (5)

TABLE VI.  $\eta'$  contribution to muon  $g - 2$  in the  $\text{VMD}_B$  model.

$\Gamma(\eta' \rightarrow \gamma\gamma)$ [keV]	$\Lambda_{\eta'}$ [GeV]	$a_\mu(\eta')/(\alpha/\pi)^3$
4.07	0.82	-0.008 655 (4)
4.07	0.85	-0.009 295 (4)
4.07	0.88	-0.009 942 (5)
4.26	0.81	-0.008 823 (4)
4.26	0.84	-0.009 475 (4)
4.26	0.87	-0.010 135 (5)
4.45	0.80	-0.008 986 (4)
4.45	0.83	-0.009 651 (5)
4.45	0.86	-0.010 323 (5)

TABLE VII. Values of  $\kappa_\phi$  and  $\beta$  in the extended model (I) for  $\pi^0$  for the various values of  $M_X$  and  $\Gamma(\pi^0 \rightarrow \gamma\gamma)$ . The error accompanying each parameter is obtained with the other parameter fixed to the best fitted value and at  $1\sigma$  confidence level.

$M_X$ [GeV]	$\Gamma(\pi^0 \rightarrow \gamma\gamma)$ [eV]	$\kappa_\phi(\pi^0)$	$\beta(\pi^0)$
$M_\rho$	7.22	$0.12^{+0.16}_{-0.12}$	$-0.0003^{+0.0215}_{-0.0218}$
$M_\rho$	7.78	$0.02^{+0.12}_{-0.10}$	$0.0035^{+0.0204}_{-0.0204}$
$M_\rho$	8.34	$-0.06^{+1.01}_{-1.35}$	$0.0065^{+0.0194}_{-0.0194}$
2.0	7.22	$0.12^{+0.15}_{-0.12}$	$-0.0005^{+0.0150}_{-0.0150}$
2.0	7.78	$0.02^{+0.12}_{-0.10}$	$0.0024^{+0.0143}_{-0.0143}$
2.0	8.34	$-0.06^{+0.10}_{-0.08}$	$0.0055^{+0.0136}_{-0.0137}$
4.0	7.22	$0.12^{+0.16}_{-0.12}$	$-0.0004^{+0.0121}_{-0.0121}$
4.0	7.78	$0.02^{+0.10}_{-0.10}$	$0.0020^{+0.0115}_{-0.0116}$
4.0	8.34	$-0.06^{+0.12}_{-0.08}$	$0.0040^{+0.0111}_{-0.0111}$
6.0	7.22	$0.12^{+0.16}_{-0.12}$	$-0.0003^{+0.0114}_{-0.0114}$
6.0	7.78	$0.02^{+0.12}_{-0.10}$	$0.0018^{+0.0108}_{-0.0108}$
6.0	8.34	$-0.06^{+0.10}_{-0.08}$	$0.0036^{+0.0104}_{-0.0104}$

TABLE VIII. Values of  $\kappa_\phi$  and  $\beta$  in the extended model (I) for  $\eta$ . The meaning of numbers are the same as in Table VII.

$M_X$ [GeV]	$\Gamma(\eta \rightarrow \gamma\gamma)$ [keV]	$\kappa_\phi(\eta)$	$\beta(\eta)$
$M_\rho$	0.42	$-0.12^{+0.11}_{-0.09}$	$0.059^{+0.022}_{-0.022}$
$M_\rho$	0.46	$-0.19^{+0.09}_{-0.07}$	$0.060^{+0.020}_{-0.020}$
$M_\rho$	0.50	$-0.25^{+0.07}_{-0.06}$	$0.061^{+0.019}_{-0.019}$
2.0	0.42	$-0.19^{+0.09}_{-0.07}$	$0.053^{+0.015}_{-0.015}$
2.0	0.46	$-0.25^{+0.07}_{-0.06}$	$0.054^{+0.014}_{-0.014}$
2.0	0.50	$-0.29^{+0.06}_{-0.05}$	$0.054^{+0.014}_{-0.014}$
4.0	0.42	$-0.16^{+0.10}_{-0.08}$	$0.040^{+0.013}_{-0.013}$
4.0	0.46	$-0.23^{+0.08}_{-0.06}$	$0.040^{+0.012}_{-0.012}$
4.0	0.50	$-0.27^{+0.06}_{-0.05}$	$0.041^{+0.011}_{-0.011}$
6.0	0.42	$-0.15^{+0.10}_{-0.08}$	$0.035^{+0.012}_{-0.012}$
6.0	0.46	$-0.21^{+0.08}_{-0.07}$	$0.035^{+0.011}_{-0.011}$
6.0	0.50	$-0.26^{+0.07}_{-0.06}$	$0.036^{+0.011}_{-0.011}$



TABLE IX. Values of  $\kappa_\phi$  and  $\beta$  in the extended model (I) for  $\eta'$ . The meaning of numbers are the same as in Table VII.

$M_X$ [GeV]	$\Gamma(\eta' \rightarrow \gamma\gamma)$ [keV]	$\kappa_\phi(\eta')$	$\beta(\eta')$
$M_\rho$	4.07	$0.30^{+0.25}_{-0.18}$	$0.015^{+0.017}_{-0.017}$
$M_\rho$	4.26	$0.22^{+0.22}_{-0.16}$	$0.016^{+0.016}_{-0.016}$
$M_\rho$	4.45	$0.15^{+0.19}_{-0.14}$	$0.017^{+0.016}_{-0.016}$
2.0	4.07	$0.25^{+0.23}_{-0.17}$	$0.015^{+0.013}_{-0.013}$
2.0	4.26	$0.17^{+0.20}_{-0.15}$	$0.016^{+0.013}_{-0.013}$
2.0	4.45	$0.11^{+0.17}_{-0.13}$	$0.016^{+0.012}_{-0.012}$
4.0	4.07	$0.25^{+0.23}_{-0.17}$	$0.012^{+0.010}_{-0.010}$
4.0	4.26	$0.17^{+0.20}_{-0.15}$	$0.012^{+0.010}_{-0.010}$
4.0	4.45	$0.11^{+0.17}_{-0.14}$	$0.013^{+0.010}_{-0.010}$
6.0	4.07	$0.27^{+0.24}_{-0.17}$	$0.010^{+0.009}_{-0.009}$
6.0	4.26	$0.19^{+0.20}_{-0.15}$	$0.010^{+0.009}_{-0.009}$
6.0	4.45	$0.13^{+0.18}_{-0.13}$	$0.011^{+0.009}_{-0.009}$

TABLE X.  $\pi^0$  pole contribution to muon  $g - 2$  in the extended model (I). The four numerals corresponding to one set of  $(\beta, \kappa_\phi)$  are the values of  $a_\mu/(10^{-2}(\alpha/\pi)^3)$  for the central value of  $\Gamma(\pi^0 \rightarrow \gamma\gamma)$ , and, from the above, for  $M_X = M_\rho$ , 2.0, 4.0 and 6.0 GeV respectively. The errors accompanying them are inferred from the uncertainty in  $\Gamma(\pi^0 \rightarrow \gamma\gamma)$ .

	$\beta(\pi^0)_{\min}$	$\beta(\pi^0)_{\text{center}}$	$\beta(\pi^0)_{\max}$
$\kappa_\phi(\pi^0)_{\min}$		$-4.391^{+0.203}_{-0.207}$	
		$-4.402^{+0.214}_{-0.220}$	
		$-4.407^{+0.220}_{-0.226}$	
		$-4.411^{+0.225}_{-0.225}$	
$\kappa_\phi(\pi^0)_{\text{center}}$	$-4.498^{+0.177}_{-0.185}$	$-4.559^{+0.206}_{-0.208}$	$-4.621^{+0.227}_{-0.231}$
	$-4.442^{+0.186}_{-0.192}$	$-4.570^{+0.212}_{-0.219}$	$-4.701^{+0.240}_{-0.245}$
	$-4.417^{+0.191}_{-0.199}$	$-4.576^{+0.216}_{-0.224}$	$-4.736^{+0.246}_{-0.252}$
	$-4.400^{+0.193}_{-0.202}$	$-4.579^{+0.223}_{-0.229}$	$-4.761^{+0.253}_{-0.257}$
$\kappa_\phi(\pi^0)_{\max}$		$-4.731^{+0.201}_{-0.208}$	
		$-4.742^{+0.211}_{-0.216}$	
		$-4.748^{+0.218}_{-0.223}$	
		$-4.751^{+0.221}_{-0.228}$	

TABLE XI.  $\eta$  contribution to muon  $g-2$  in the extended model (I). The numbers corresponding to one set of  $(\beta, \kappa_\phi)$  have the meaning similar to those of Table X.

	$\beta(\eta)_{\min}$	$\beta(\eta)_{\text{center}}$	$\beta(\eta)_{\max}$
$\kappa_\phi(\eta)_{\min}$		$-0.995^{+0.063}_{-0.062}$	
		$-1.119^{+0.082}_{-0.083}$	
		$-1.154^{+0.085}_{-0.086}$	
		$-1.174^{+0.087}_{-0.087}$	
$\kappa_\phi(\eta)_{\text{center}}$	$-0.990^{+0.055}_{-0.056}$	$-1.031^{+0.063}_{-0.062}$	$-1.074^{+0.071}_{-0.070}$
	$-1.067^{+0.072}_{-0.073}$	$-1.146^{+0.083}_{-0.083}$	$-1.229^{+0.094}_{-0.094}$
	$-1.090^{+0.074}_{-0.075}$	$-1.182^{+0.086}_{-0.085}$	$-1.278^{+0.098}_{-0.098}$
	$-1.104^{+0.075}_{-0.076}$	$-1.202^{+0.087}_{-0.088}$	$-1.308^{+0.101}_{-0.100}$
$\kappa_\phi(\eta)_{\max}$		$-1.069^{+0.064}_{-0.064}$	
		$-1.173^{+0.083}_{-0.084}$	
		$-1.210^{+0.086}_{-0.087}$	
		$-1.230^{+0.088}_{-0.088}$	

TABLE XII.  $\eta'$  contribution to muon  $g - 2$  in the extended model (I). The numbers corresponding to one set of  $(\beta, \kappa_\phi)$  have the meaning similar to those of Table X.

	$\beta(\eta')_{\min}$	$\beta(\eta')_{\text{center}}$	$\beta(\eta')_{\max}$
$\kappa_\phi(\eta')_{\min}$		$-0.842^{+0.018}_{-0.018}$	
		$-0.859^{+0.021}_{-0.021}$	
		$-0.872^{+0.021}_{-0.021}$	
		$-0.879^{+0.022}_{-0.022}$	
$\kappa_\phi(\eta')_{\text{center}}$	$-0.887^{+0.016}_{-0.016}$	$-0.897^{+0.018}_{-0.018}$	$-0.906^{+0.021}_{-0.021}$
	$-0.878^{+0.017}_{-0.017}$	$-0.910^{+0.021}_{-0.021}$	$-0.942^{+0.025}_{-0.025}$
	$-0.881^{+0.018}_{-0.018}$	$-0.923^{+0.022}_{-0.022}$	$-0.965^{+0.026}_{-0.026}$
	$-0.884^{+0.018}_{-0.018}$	$-0.930^{+0.022}_{-0.022}$	$-0.977^{+0.027}_{-0.027}$
$\kappa_\phi(\eta')_{\max}$		$-0.953^{+0.019}_{-0.019}$	
		$-0.962^{+0.021}_{-0.021}$	
		$-0.975^{+0.022}_{-0.022}$	
		$-0.982^{+0.023}_{-0.023}$	

TABLE XIII.  $\beta$  and  $\kappa_\phi$  in the extended model (II) for  $\pi^0$  for the various values of  $\Gamma(\pi^0 \rightarrow \gamma\gamma)$ . The error accompanying each parameter is obtained with the other parameter fixed to the best fitted value and at  $1\sigma$  confidence level.

$\Gamma(\pi^0 \rightarrow \gamma\gamma)$ [eV]	$\kappa_\phi(\pi^0)$	$\beta(\pi^0)$
7.22	$0.13_{-0.12}^{+0.16}$	$-0.004_{-0.043}^{+0.042}$
7.78	$0.07_{-0.10}^{+0.12}$	$0.011_{-0.043}^{+0.043}$
8.34	$-0.09_{-0.08}^{+0.09}$	$0.028_{-0.044}^{+0.047}$

TABLE XIV.  $\beta$  and  $\kappa_\phi$  in the extended model (II) for  $\eta$ . The meaning of numbers is the same as in Table XIII.

$\Gamma(\eta \rightarrow \gamma\gamma)$ [keV]	$\kappa_\phi(\eta)$	$\beta(\eta)$
0.42	$-0.28_{-0.05}^{+0.06}$	$0.30_{-0.07}^{+0.08}$
0.46	$-0.30_{-0.05}^{+0.05}$	$0.27_{-0.07}^{+0.08}$
0.50	$-0.32_{-0.04}^{+0.05}$	$0.24_{-0.06}^{+0.07}$

TABLE XV.  $\beta$  and  $\kappa_\phi$  in the extended model (II) for  $\eta'$ . The meaning of numbers is the same as in Table XIII.

$\Gamma(\eta' \rightarrow \gamma\gamma)$ [keV]	$\kappa_\phi(\eta')$	$\beta(\eta')$
4.07	$-0.31_{-0.05}^{+0.05}$	$0.20_{-0.03}^{+0.03}$
4.26	$-0.30_{-0.05}^{+0.05}$	$0.19_{-0.03}^{+0.03}$
4.45	$-0.28_{-0.05}^{+0.05}$	$0.17_{-0.03}^{+0.03}$

TABLE XVI.  $\pi^0$  pole contribution to  $a_\mu/(10^{-2}(\alpha/\pi)^3)$  in the extended model (II). The errors accompanied with them are inferred from the uncertainty in  $\Gamma(\pi^0 \rightarrow \gamma\gamma)$ .

	$\beta(\pi^0)_{\min}$	$\beta(\pi^0)_{\text{center}}$	$\beta(\pi^0)_{\max}$
$\kappa_\phi(\pi^0)_{\min}$		$-4.386^{+0.193}_{-0.183}$	
$\kappa_\phi(\pi^0)_{\text{center}}$	$-4.457^{+0.186}_{-0.189}$	$-4.559^{+0.196}_{-0.188}$	$-4.662^{+0.196}_{-0.187}$
$\kappa_\phi(\pi^0)_{\max}$		$-4.736^{+0.201}_{-0.191}$	

TABLE XVII.  $\eta$  pole contribution to  $a_\mu/(10^{-2}(\alpha/\pi)^3)$  in the extended model (II).

	$\beta(\eta)_{\min}$	$\beta(\eta)_{\text{center}}$	$\beta(\eta)_{\max}$
$\kappa_\phi(\eta)_{\min}$		$-0.582^{+0.047}_{-0.048}$	
$\kappa_\phi(\eta)_{\text{center}}$	$-0.677^{+0.053}_{-0.052}$	$-0.638^{+0.049}_{-0.050}$	$-0.600^{+0.046}_{-0.047}$
$\kappa_\phi(\eta)_{\max}$		$-0.697^{+0.051}_{-0.051}$	

TABLE XVIII.  $\eta'$  pole contribution to  $a_\mu/(10^{-2}(\alpha/\pi)^3)$  in the extended model (II).

	$\beta(\eta')_{\min}$	$\beta(\eta')_{\text{center}}$	$\beta(\eta')_{\max}$
$\kappa_\phi(\eta')_{\min}$		$-0.824^{+0.042}_{-0.035}$	
$\kappa_\phi(\eta')_{\text{center}}$	$-0.844^{+0.028}_{-0.016}$	$-0.872^{+0.038}_{-0.033}$	$-0.893^{+0.045}_{-0.038}$
$\kappa_\phi(\eta')_{\max}$		$-0.915^{+0.036}_{-0.032}$	

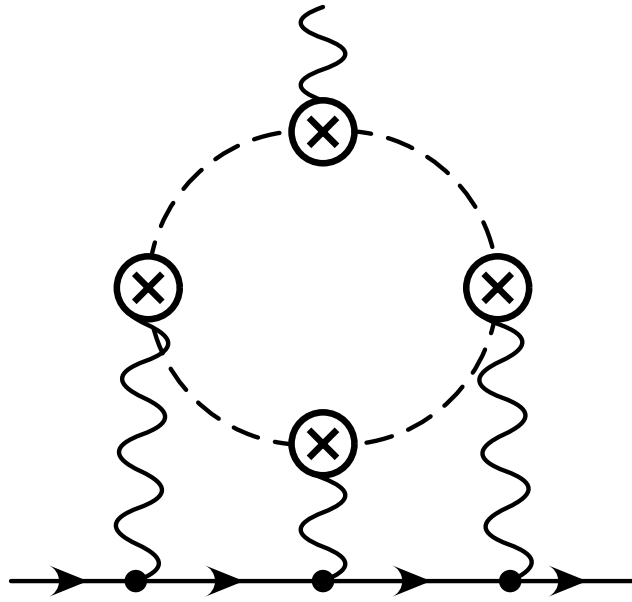
## FIGURES

FIG. 1. Leading diagrams in the chiral perturbation and  $1/N_c$  expansion which contribute to the hadronic light-by-light scattering effect on the muon anomaly: (a) pion-loop diagram, (b) pseudoscalar pole diagram, (c) quark-loop diagram. Solid and wavy lines represent muon and photon respectively. Dotted line in (a) corresponds to the charged pseudoscalar meson while dotted line connecting the two blobs in (b) corresponds to the neutral one. The closed solid line in (c) represents the quark loop. These diagrams are typical ones in respective classes.

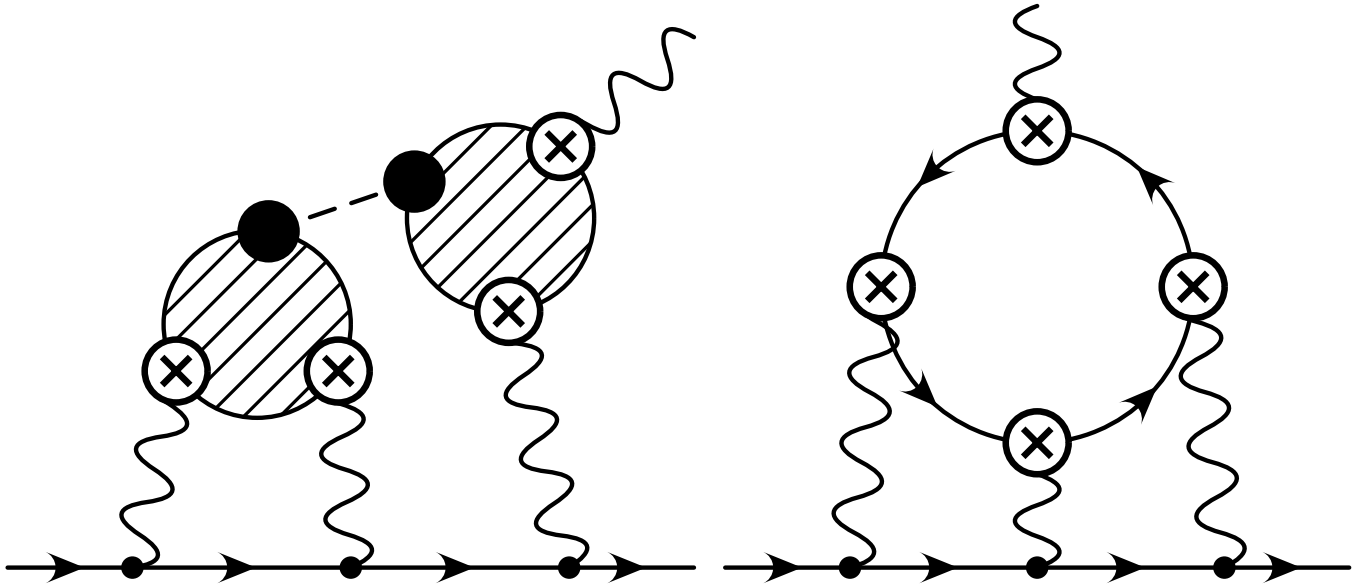
FIG. 2. Pseudoscalar pole diagrams. Dotted line between the two blobs represents the propagation of neutral pseudoscalar meson.

FIG. 3. Comparison of various theoretical form factors of  $\Gamma(\pi^0 \rightarrow \gamma\gamma^*)$  with the experimental data. Solid line corresponds to the VMD model ( $b_1$ ) while dashed line ( $b_2$ ) and dot-dashed lines ( $b_3$ ) correspond to the QTL model and the QTL model supplemented by the VMD model, respectively.

FIG. 4. Comparison of the various theoretical asymptotic behavior of form factors of  $\Gamma(\pi^0 \rightarrow \gamma\gamma^*)$  with the experimental data. Three straight lines, from the above, are the Brodsky-Lepage (BL), OPE and the Gerard-Lahna (GL) predictions, respectively. The curve representing the Brodsky-Lepage interpolation formula (2.13) is also shown for comparison.



(a)



(b)

(c)

FIG. 1



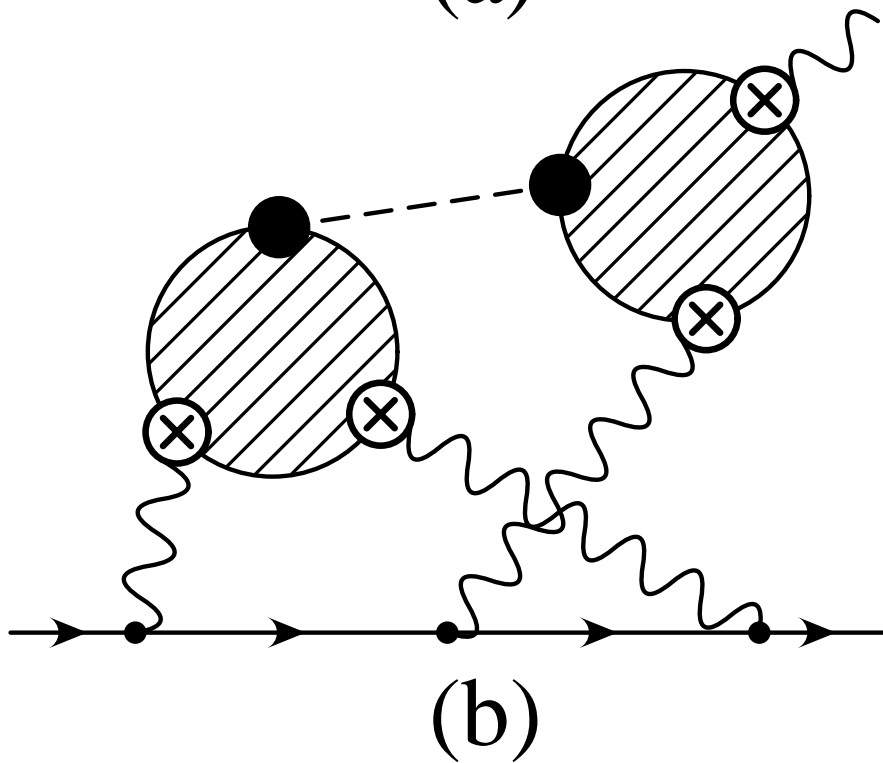
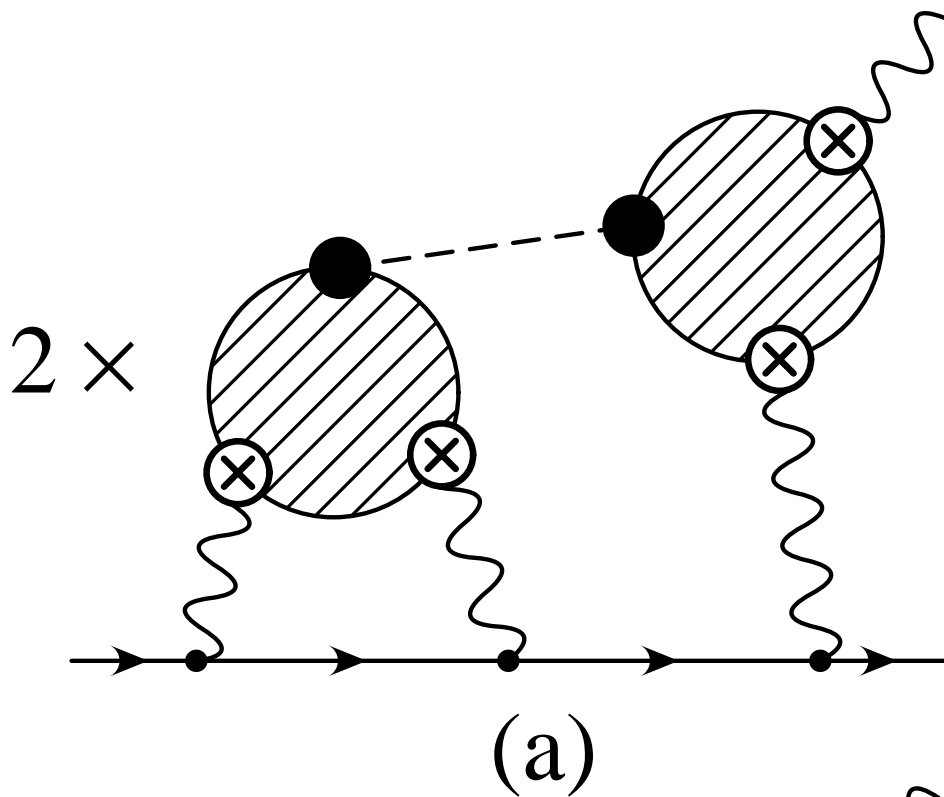


FIG. 2

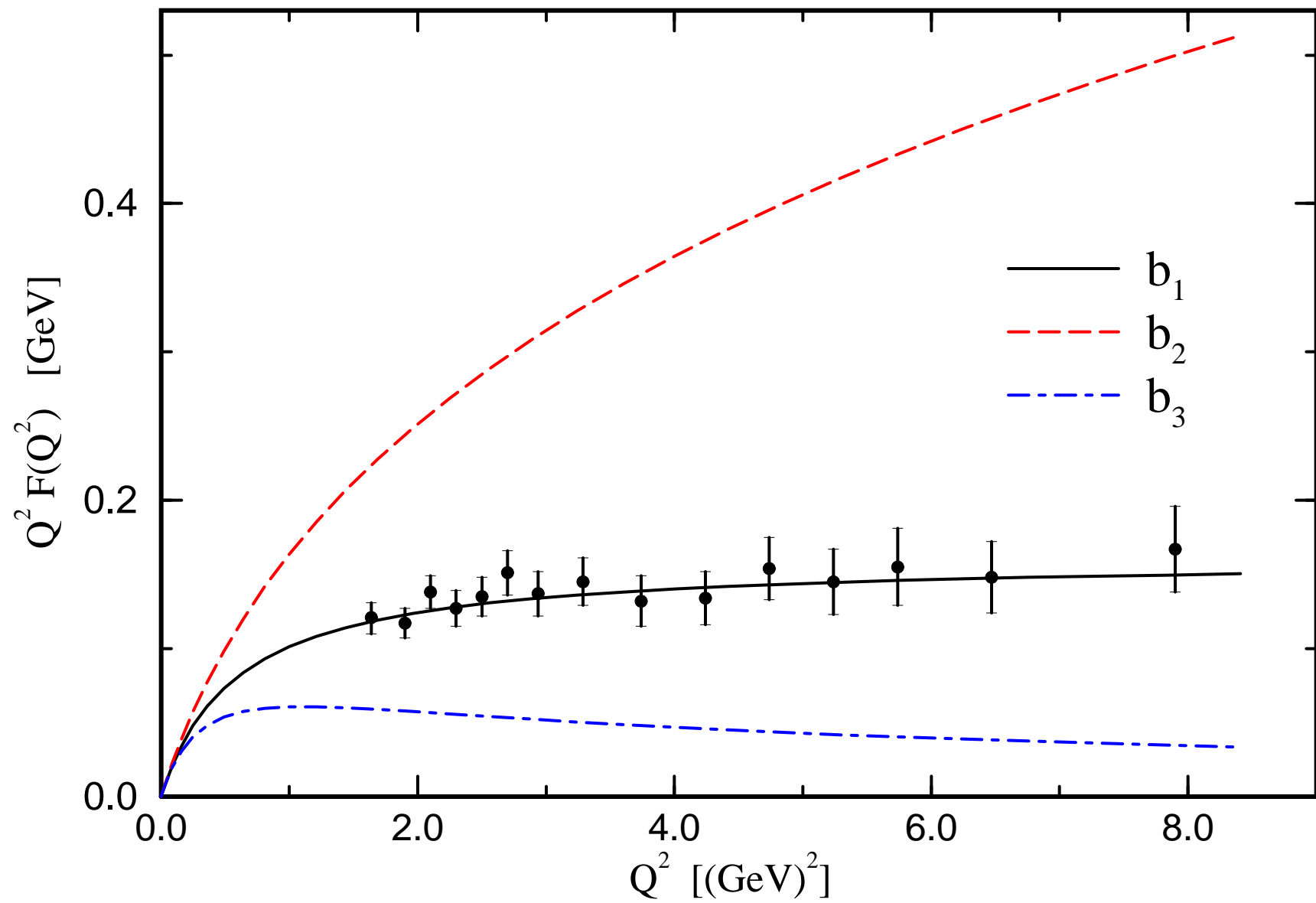


FIG. 3

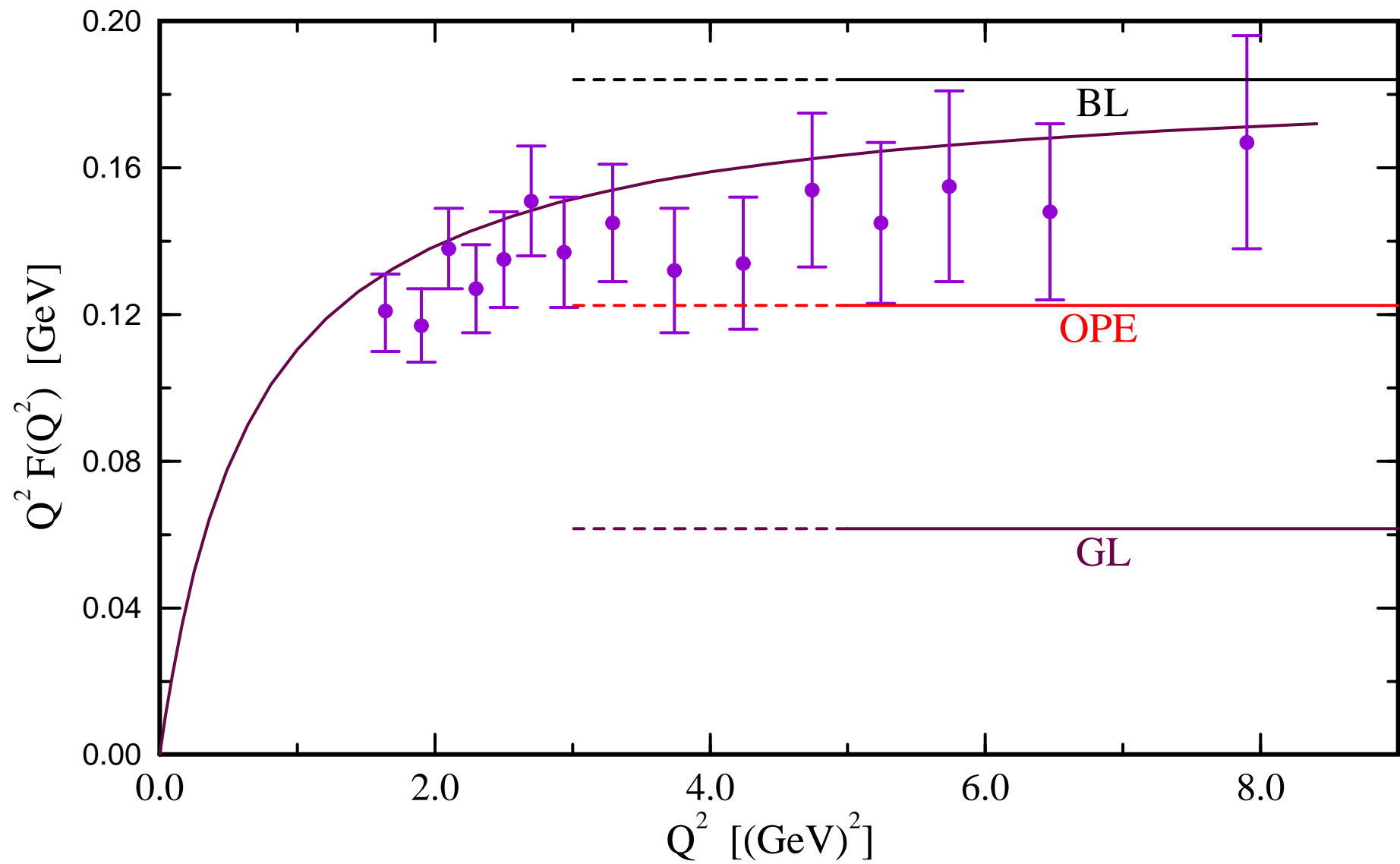


FIG. 4